Thermochimica Acta 499 (2010) 128–132

Contents lists available at ScienceDirect

Thermochimica Acta

journal homepage: www.elsevier.com/locate/tca

Construction, calibration and testing of a decimeter-size heat-flow calorimeter

Wu-Shou Zhang*

Beijing National Laboratory for Molecular Sciences, Key Laboratory of Colloid, Interface and Chemical Thermodynamics, Institute of Chemistry, Chinese Academy of Sciences, P.O. Box 2709, Beijing 100190, China

ARTICLE INFO

Article history:
Received 24 September 2009
Received in revised form
12 November 2009
Accepted 27 November 2009
Available online 3 December 2009

Keywords:
Calorimetry
Heat-flow calorimeter
Heat-conduction calorimeter
Thermo-kinetics

ABSTRACT

A heat-flow calorimeter was designed and built. Its measurements are 26 cm × 26 cm × 26 cm (17.6 dm^3). 18,796 thermocouples are used to measure the heat-flow from the vessel walls to the outer walls, for which temperature is controlled within 0.01 °C from 0 to 100 °C by a refrigerating/heating circulator. Homogeneity of temperature in the measuring vessel is improved by a fan with constant power. The calibration was performed with an electric heater, with input power up to 50 W. The device constant is 5.8954 ± 0.0025 W V^{-1}; the time constant is 501.7 ± 3.2 s; the uncertainty is 0.6% at 2 W to 0.06% at 50 W. Nonlinearity of this calorimeter is analyzed. The calorimeter can be utilized for studies of kinetics and thermodynamics of physical, chemical and biological systems of decimeter-size. A Sony 26650 Li-ion rechargeable battery was tested with this device during charging and discharging, and an electrolytic cell with Pd-D_2O was also tested with this device.

1. Introduction

Heat-flow calorimeters (HFCs), or heat-conduction calorimeters, are widely utilized for measurements of power and enthalpy change during physicochemical reactions in basic research and technical applications. Among these sorts of devices, Tian–Calvet microcalorimeters are frequently used for tiny samples (<10^1 cm^3) and low powers (≪10^{-1} W) [1]. For larger samples and higher power, other types are more suitable. One option is the Seebeck Envelope Calorimeter (SEC) made by Thermonetics Corporation [2]; however, this sort of device has some intrinsic defects in the author's experience [3]:

(1) The heat insulator around the calorimeter is insufficient; thus the baseline and output signals oscillate daily with the ambient temperature and drift with human activities.
(2) The device constant, the quotient of thermal power P to the output emf (electromotive force) of thermoelectric pile V, $D_1 = P/V$, is unstable. The author found that it shifted by 20% in three months; the SEC had to be calibrated before and after every measurement.
(3) The isothermality is not good. Although Tian–Calvet microcalorimeters are semi-isothermal, the temperature difference between the sample under test and its environment is generally very small (<10^{-4} °C) because of small sizes and low powers of samples. However, the isothermality may become a problem for samples of decimeter-size due to slow heat transfer in samples, and/or across the barrier (interlayer between measuring vessel and outer layer at constant temperature, including the thermoelectric pile and junction parts). For example, the thermal conductance of the barrier σ = 2.44 W °C^{-1} for a Thermonetics SEC, this means the temperature difference reaches about 4.1 °C for 10 W of thermal power liberated. This non-isothermality makes the working temperature differ prominently from the set value and this disagreement should be avoided or reduced.
(4) The nonlinearity of the device constant is remarkable. The device constant of Thermonetics SEC is 187.4 W V^{-1} at 1 W and 186.0 W V^{-1} at 20 W in linear approximation. This should be partly caused by the non-isothermality of this device.

In the literature, there were also reports on large-scale custom-made heat-flow calorimeters for special purposes [4,5]. These also had, to some extent, defects like the Thermonetics SEC. Some researchers used mass flow calorimeters [6–9]; however, this type of calorimeter has more parameters to determine the power than the Tian calorimeter. In this paper, we will describe a new heat-flow calorimeter with large measuring volume and a wide power range. Its merits are simplicity, stability, accuracy, and fewer defects than the Thermonetics SEC. It will be useful in research on thermokinetics and thermal behavior of systems in decimeter-size.

2. Construction of calorimeter

Fig. 1 shows a schematic of the HFC. The calorimeter core consists of two embedded boxes made of an aluminum alloy. The

* Tel.: +86 10 6255 4276; fax: +86 10 6255 9373.
E-mail address: wszhang@iccas.ac.cn.

0040-6031/$ – see front matter © 2009 Elsevier B.V. All rights reserved.
doi:10.1016/j.tca.2009.11.013

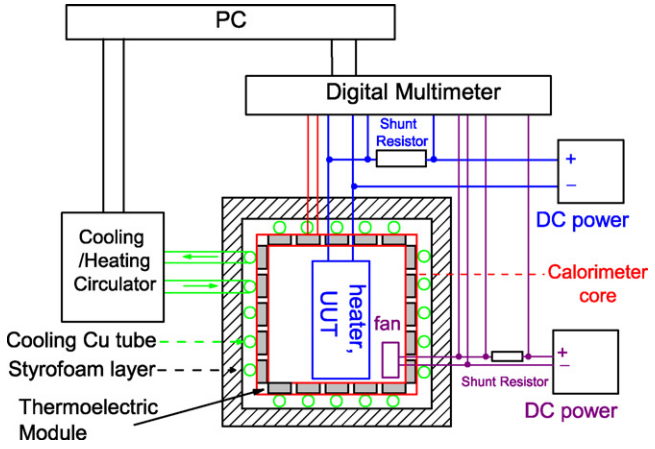

Fig. 1. Schematic of the heat-flow calorimeter.

inner box is the measuring vessel with interior dimensions of 26 cm × 26 cm × 26 cm (17.576 dm^3). The thicknesses of the inner and outer box walls are 4 and 6 mm, respectively. Thermoelectric modules (TM, 5.4 mm × 40 mm × 40 mm) each with 127 thermocouples, are mounted between the inner and outer walls with screws. Thermal conductive silicone is wiped on both sides of each TM for improving thermal conductivity. 25 TMs are distributed uniformly on each wall except for 2 facing sidewalls which have 24 TMs because there is one hole in the center of each wall. Altogether, 148 TMs with a total of 18,796 thermocouples are used in this calorimeter. All TMs are connected in series. The heat flow released or absorbed during experiments is proportional to the measured emf of TMs.

The two holes (ϕ = 2 cm) in the two sidewalls mentioned above permit multi-functionality of this calorimeter, i.e., controls of mechanical, pressure and circulation of working fluid, measurements of temperature, internal resistance and voltage of the unit-under-test (UUT). The thermal emf of the calorimeter and other signals of UUT are measured with a Keithley 2000 multimeter which is connected to a PC through a GPIB card, to automatically register the data obtained using software.

The outer aluminum alloy box is wired with copper tubing (ϕ_{in} = 8 mm, ϕ_{out} = 10 mm). Thermal conductive adhesive (Good Friend®, working temperature = −3 to 235 °C, thermal conductivity > 1.2 W m^{-1} $°C^{-1}$) is used to mount the copper tubing and the aluminum alloy walls. The outlet of copper tubing is connected with the hose of a refrigerating/heating circulator (PolyScience 9112). The temperature range of this circulator is −20 to 200 °C; the temperature stability is ±0.01 °C, the flow rate of the working fluid is 15–22 dm^3 min^{-1}. The inlet of the copper tubing is connected with a small cylindrical thermostatic bath (ϕ_{in} 20 mm × h_{in} 50 mm); a remote temperature probe of the circulator is placed in it. This arrangement of temperature probe ensures the fluctuation of ambient temperature does not affect the calorimetry. The inlet of the small bath is connected to the circulator with another hose. All these hoses are wrapped with foam tubing to prevent heat losses.

The calorimeter core is placed in a larger box with interior dimension of 70 cm × 70 cm × 70 cm. Heat insulation materials fill in the gap between these two boxes. The inner surface of the large box is covered with aluminum film, and the inner and outer walls of the calorimeter core are connected with ground to avoid electromagnetic interference.

3. Calibration of calorimeter

Before calibration, we tested the baseline stability (noise) with two modes of temperature control. One is remote control as described above; another is local control, i.e. the temperature probe was in the circulation bath but not in the HFC. We found the latter mode gave more stable baselines than the former in a short time range and some ambient temperature dependent baselines in a long time range, as expected. For example, the baseline was −1.06 ± 1.23 mV at night (10 h) and −1.15 ± 2.95 mV for a 24 h day (bath temperature was 25.00 °C; room temperature was 22–26 °C). The remote control gave a baseline of 8.07 ± 3.81 mV over 32 h (bath temperature was 25.00 °C; room temperature was 28–31 °C). For an ideal calorimeter, the baseline signal should be zero or very small; however, heat exchanges between the calorimeter and its environment cause the HFC to have a non-zero baseline, and its value drifts slightly with room temperatures. Its magnitude can be stabilized through control of room temperature using an air conditioner.

The calibration was conducted with a 3.6 Ω electric heater. The heater is made of Tophet® alloy A wire (ϕ 0.3 mm) wound around a cylindrical heat sink with fins, which were located at the center of the measuring vessel. This configuration ensures a uniform distribution of temperature in air and between the heat sink and air. The heater was connected to a DC power source (ITECH, IT6921). The four-wire Kelvin bridge method was used to eliminate lead resistance in the measurements. Applied current was measured with a 0.1 Ω (±0.01%) standard resistor as shunt.

A Sanyo Denki brushless fan (12 V × 0.21 A, 2.5 W) with another DC power supply (ITECH, IT6322), and a 1 Ω (±0.01%) shunt was used to homogenize the temperature distribution in the measuring vessel as illustrated in Fig. 1. The power of the fan was also measured in a similar manner.

The calorimeter was calibrated from 0.1 to 50 W; it gave good linearity between thermal power and responses. One series of calibration is shown in Fig. 2. These results are simulated by a quadratic equation:

$$P = D_0 + D_1V + D_2V^2 = -0.0451 \pm 0.0046 + (5.8954 \pm 0.0025)V - (0.0019 \pm 0.0003)V^2 \quad (1)$$

with the residual sum of squares $\chi^2 = 1.2 \times 10^{-4}$ and the adjusted R-square $R^2 = 1$. Where P is the input power in Watts, and V is the output emf in Volts. This simulation gives the uncertainty of 6.9% at 0.1 W, 0.6% at 2 W and 0.06% at 50 W. The time constant of the HFC, τ = 501.7 ± 3.2 s.

In Eq. (1), the first term D_0 corresponds to the baseline signal, it can be removed by deducting the baseline from the output emf and its value does not affect the magnitudes of D_1 and D_2. The device constant in the second term, D_1 = 5.8954 ± 0.0025 W V^{-1}, or about

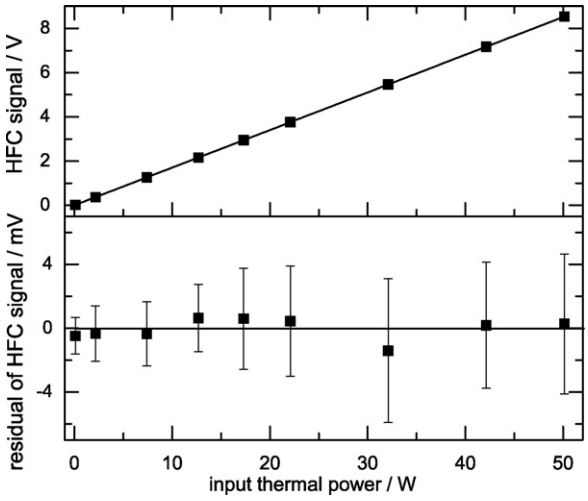

Fig. 2. Calibration results of calorimeter with an electric heater at 25.00 ± 0.01 °C.

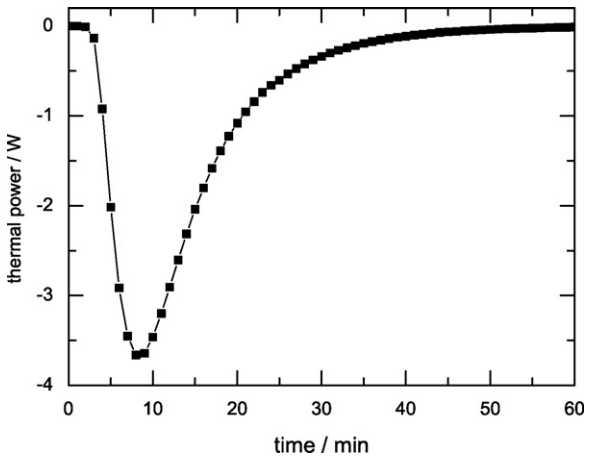

Fig. 3. Power pulse when the temperature of outer wall increased from 25 to 26 °C, the corresponding heat capacity of the calorimeter is 5.30 ± 0.02 kJ °C^{-1}.

30 times more sensitive than the Thermonetics SEC in Ref. [3]. The device constant did not change more than 0.6% in two years. The quadratic term is very small, $D_2V/D_1 = 0.3\%$ at 50 W. By comparison, the contribution of nonlinearity: $D_2V/D_1 = 3\%$ for a Thermonetics SEC [3] and 2% in Ref. [4] when the thermal power is extrapolated to 50 W.

The effect of thermal heterogeneity in the measuring vessel on the calorimetry was tested. A heater made of straight Tophet® alloy A wire with resistance of 6 Ω clung to one sidewall when power to the fan was off. The resulting device constant was 6.1071 ± 0.0176 W V^{-1} up to 24 W, which was 3.5% greater than 5.8954 ± 0.0025 W V^{-1}. This location dependence of the device constant means uniform distribution of temperature in the measuring vessel is important for precise measurements of thermal power.

The effective heat capacity of the calorimeter was determined by changing its outer wall temperature, $C = 5.30 \pm 0.02$ kJ °C^{-1} from 25 to 26 °C, as shown in Fig. 3. In measurements of heat capacity of samples, this figure is the background of the actual value and it should be deducted from the measured quantity. The full-width at the half-maximum of the pulse in Fig. 3 is 658.4 s, which is also the response time of the HFC. The decaying part is simulated using an exponential function. The corresponding time constant is 543.9 ± 9.0 s. These two time constants are longer than τ due to thermal processes in the outer walls being included here. Although the above three different characteristic time constants have different values, they are close to each other and in the range of 500–660 s.

According to Ref. [1], the thermal conductance of the barrier in a Tian calorimeter is:

$$\sigma = \frac{C}{\tau} = 10.56 \pm 0.11 \text{ W °C}^{-1} \quad (2)$$

The measured value of $\sigma = 11.65 \pm 0.25$ W °C^{-1} when thermal power changed from 2.13 to 12.58 W at 25.00 °C. These two values are the same within the error of 10%. Their difference arises from the measured τ including not only heat capacity in a Tian calorimeter but also thermal diffusion in HFC as mentioned above. This reason makes the measured thermal conductance greater than the theoretical value in Eq. (2). The σ for HFC is about 5 times that of a Thermonetics SEC. This means that this device has better isothermality than the latter. Generally speaking, there is a balance between sensitivity and isothermality for any calorimeter; however, the HFC has better both sensitivity and isothermality than a Thermonetics SEC.

4. Nonlinearity of the calorimeter

The HFC described here, compared with a Tian calorimeter, has larger measuring volume and higher power. This makes the nonlinearity of P–V relation prominent when the thermal power is high, as shown in Eq. (1). This phenomenon can be understood from the temperature dependence of Seebeck effects. For simplicity, the Seebeck coefficient can approximate to:

$$\alpha \approx \alpha_0 + \alpha_1 \Delta T \quad (3)$$

For most thermocouples, α increases with T around room temperature [10], i.e. $\alpha_1 > 0$. Therefore the output emf of the HFC is:

$$V = N\alpha\Delta T \approx N\alpha_0\Delta T + N\alpha_1\Delta T^2 \quad (4)$$

where $N = 18{,}796$, the number of thermocouples used in HFC. ΔT is the temperature difference across the thermal barrier. Because the thermal power is proportional to the temperature difference:

$$P = \sigma\Delta T \quad (5)$$

Eq. (4) can be expressed as

$$V \approx \frac{N\alpha_0}{\sigma}P + \frac{N\alpha_1}{\sigma^2}P^2 \quad (6)$$

Solving P and expanding it to the second order gives:

$$P \approx \frac{\sigma}{N\alpha_0}V - \frac{\sigma\alpha_1}{N^2\alpha_0^3}V^2 \quad (7)$$

Two constants in Eq. (3) can be obtained by combining Eqs. (1) and (7) and parameters above: $\alpha_0 = 0.1051 \pm 0.0023$ mV °C^{-1} and $\alpha_1 = 67 \pm 16$ nV °C^{-2}. Besides HFC here, Thermonetics SEC and Storms' calorimeter also exhibited negative values of D_2 in quadratic approximations [3,5].

Referring to Eq. (7), the ratio of the quadratic term to the linear term in Eq. (1) is:

$$\frac{D_2V^2}{D_1V} = \frac{\alpha_1 V}{N\alpha_0^2} \approx \frac{\alpha_1}{\alpha_0}\frac{P}{\sigma} \quad (8)$$

in the first order approximation. It is 0.27% at 50 W here, one order less than that reported in Refs. [3–5]. Eq. (8) predicts that an ideal linearity of a HFC relies on a small temperature dependence of the Seebeck coefficient (low value of α_1/α_0) and good thermal conductance of the calorimeter (high value of σ).

5. Test of the calorimeter

5.1. Thermal behavior of a rechargeable battery

Calorimetry is a useful tool for measurements of heat dissipation during charge/discharge of rechargeable batteries [11,12]. The large volume and high power range of this calorimeter make it suitable for studying thermal behaviors of batteries and battery modules. A Sony 26650, MFC07P, 2700 mAh, 3.7 V, Li-ion rechargeable battery (ϕ 26 mm × 65 mm) was used to test the calorimeter. The battery was placed on a foam block, and one K-type thermocouple was attached on the top center of its cylindrical surface to measure temperature. The fan in the HFC was off in the test to simulate the heat transfer of natural convection. The induced error of thermal power measurement is less than 3.5%, as discussed in Section 3. For evaluating the battery, over-charge and over-discharge were applied in the experiments.

The heat dissipation during charge and discharge in the galvanostatic mode with 0.9 A ($C/3$) is shown in Fig. 4 and Table 1. The surface temperature of the battery decreases in the initial period of charge (see insert to Fig. 4(a)); this heat absorption is induced by the entropy change and it would be observed if the charging current was much lower than here, as illustrated in Ref. [12]. The

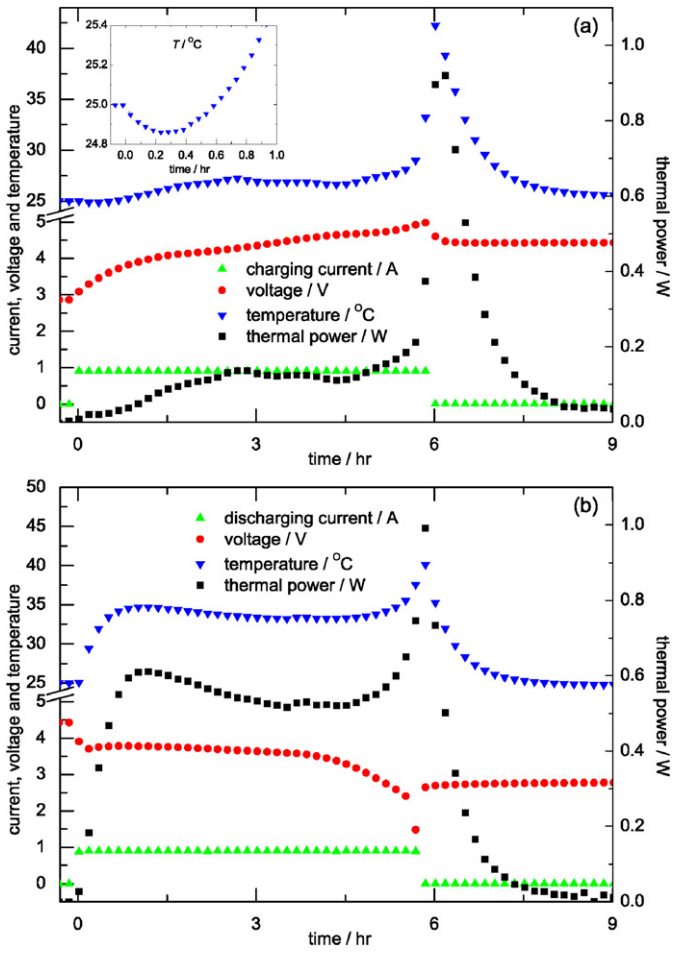

Fig. 4. Heat dissipation of a Sony 26650 Li-ion rechargeable battery during charge (a) and discharge (b) at constant current of 0.9 A (*C*/3), 25 °C. The insert shows that temperature decreases in the initial period of charging.

thermal power was less than 0.2 W before the quantity of charge reached 4500 mAh. The heat released increased sharply when the actual charge quantity approached 5400 mAh (2 times the nominal capacity). It appeared that the battery would be in thermal run-away, the charging was stopped intentionally.

The discharge was conducted the next day after charging with the same current, 0.9 A (*C*/3), and the thermal power released was always about 0.6 W. The thermal power and temperature increased sharply when the discharge electric quantity approached 4950 mAh (11/12 of the charged capacity in the previous day), and the discharge was then stopped intentionally.

By comparison of parameters in charge and discharge processes, it is found that the thermal power during discharge is about 2.5 times of that in charge. The efficiency in discharge is lower than that in charge as shown in Table 1.

Table 1
Summary of heat dissipation during charge and discharge of a Sony 26650 Li-ion battery.

	Q (mAh)	E (kJ)	H (kJ)	ε	$\bar{P}$(W)
Charge	5 398	83.74	5.39	94%	0.25
Discharge	5 178	64.07	13.25	83%	0.64

Note: Q is the quantity of charge; E is the electrical energy; H is heat released; $\varepsilon = (E - H)/E$ for charge and $\varepsilon = E/(E + H)$ for discharge, the efficiency; $\bar{P}$ is the average thermal power.

5.2. Calorimetry of Pd-D_2O electrolytic cell

Thermal power is less than 1 W in the above experiments. Results will now be presented on an electrochemical process that produced power one order higher than that of the Li-ion battery. The primary purpose of these experiments was to repeat Fleischmann–Pons effects as was done in one earlier work [3]; however, some trivial results demonstrated the accuracy of this calorimeter. One example of these will be presented here.

The electrolytic cell is a cylinder of borosilicate glass (ϕ_{in} 42 mm × ϕ_{out} 45 mm × h 142 mm). A PTFE male cap is tapered from a hexagonal prism with side length 32 mm and thickness 13 mm at the top, and ϕ 41 mm × 24 mm at the bottom. A groove of 4 mm width and 2.5 mm depth was made for O-ring in the middle of bottom part. The O-ring (ϕ_{in} = 31.5 mm, width = 3.55 mm) made of nitrile butadiene rubber (NBR, resistant to acid) is used to seal the top cap against the top inner wall of glass cylinder. The top cap has two holes, 1 mm diameter each and 20 mm apart, for the electrode lead wires. A PTFE plate (ϕ 41 mm × 8 mm) is used to suspend the recombination catalyst above the electrode. It has 57 holes of ϕ 2 mm to pass gases (D_2 and O_2) and vapors (D_2O). A PTFE rod (ϕ 6 mm × 40 mm) is fastened to the perforated plate and the top cap. This ensures that the perforated plate is at a fixed distance above the electrolyte.

The cathode is palladium foil, 11 mm × 31 mm × 0.5 mm, the anode is platinum foil, 31 mm × 43 mm × 0.02 mm. Two electrode lead wires made of Pt (ϕ 0.8 mm × 145 mm) are covered with heat-shrink teflon tubing. The electrolyte contains 51.5 g of heavy water mixed with 8.115 g of D_2SO_4. Catalyst (3 g), which contains 0.5% Pt on 1/8 inch diameter alumina pellets, is used in the cell to recombine the D_2 and O_2 which evolves during electrolysis. O_2 gas at 1 atmosphere was flowed into the cell to accelerate catalysis. A metal frame was used to clamp the PTFE cap onto the cell. These arrangements ensure that the electrolytic cell is a closed system. Energy exchange occurs only during electrolysis.

The electrolysis was carried out in galvanostatic mode (3 A) using a DC power source (ITECH IT6921), which was also used during calibration. Fig. 5 shows the input electrolytic power and output thermal power. The input and output powers are 8.9556 ± 0.0029 and 8.9552 ± 0.0264 W, respectively, during the stable period (5–8 h of electrolysis time). They are consistent with each other within 0.004%, although the calorimetric error is 0.29%.

The input and output energies are 262.38 ± 0.05 and 261.83 ± 0.88 kJ, respectively. Before and after electrolysis, the cell was weighed with Mettler PM1200; the mass loss in this run was

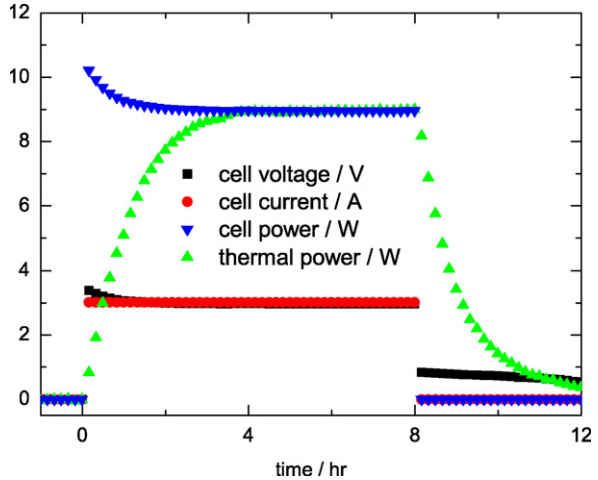

Fig. 5. Comparison of input electrolytic power with output thermal power of a Pd-D_2O cell. The fan's power is deducted from the total power.

0.022 g. If this loss was caused by poor catalytic recombination, the corresponding energy correction is 0.33 ± 0.03 kJ. The output energy after correction is 262.16 ± 0.90 kJ; the resulting excess energy is -0.22 ± 0.90 kJ, corresponding to $(-0.08 \pm 0.34)\%$ of the input energy. It means there was no excess heat produced in the electrolytic cell and this calorimeter gave good accuracy (better than 0.1%) at power around 9 W running for 8 h.

6. Discussions

Besides applications in battery studies presented in Section 5.1, side reactions and their mechanisms in batteries can also be studied using this calorimeter. For modules of Ni-MH rechargeable batteries, this HFC can be used to evaluate the self-discharge directly through thermal power measurement. Furthermore, this calorimeter can be utilized in safety and abuse evaluations of Li-ion rechargeable battery using methods of punctuation and short-circuit. The heat released during such processes can be measured quantitatively through making a mechanical or electric link between the battery in the measuring vessel and control parts outside of HFC.

At the same time, this calorimeter can be used for other samples or systems in decimeter-size, e.g. fuel cells, animals, plants and radioactive materials, to study their physiochemical, biological and nuclear processes through thermal power measurements.

On the basis of the construction and application of HFC presented here, its advantage and uniqueness of large volume and wide power range are obvious by comparison with a Tian–Calvet calorimeter. Of course, the twin-cell design used in the Tian–Calvet calorimetry [1] cannot be applied directly here due to the large volume of the measuring vessel. By comparison with a Thermonetics SEC, its stable device constant, good isothermality and linearity are markedly superior. At the same time, there are still defects in this HFC; one of them is the prominent baseline signal especially when the thermal power is less than 0.1 W. This problem will be solved in the next version of HFC.

Acknowledgments

Thanks to Prof. Z.-L. Zhang and J. Dash for valuable discussions. This work was supported by NSFC (20673129 & 20973185), 973 Program of MOST in China (2009CB226113), Innovation Project of CMS (CMS-CX200816) and SRF for ROCS, SEM.

References

[1] E. Calvet, H. Prat, Recent Progress in Microcalorimetry, Pergamon Press, Oxford, 1963 (Chapters 3 and 4).
[2] Thermonetics Corporation, 7834 Esterel Drive, La Jolla, CA 92037, USA, http://www.thermoneticscorp.com.
[3] W.-S. Zhang, J. Dash, Q. Wang, Condensed matter nuclear science, in: A. Takahashi, K.-I. Ota, Y. Iwamura (Eds.), Proc. 12th Int. Conf. Cold Fusion, Yokohama, Japan, November 27–December 2, 2005, World Scientific Pub., Singapore, 2006, p. 86.
[4] A.A. Pesaran, D.J. Russell, J.W. Crawford, R. Rehn, E.A. Lewis, Proceedings of the 13th Annual Battery Conference: Applications and Advances, Long Beach, California, January 13–16, 1998, p. 127.
[5] E. Storms, Condensed matter nuclear science, in: A. Takahashi, K.-I. Ota, Y. Iwamura (Eds.), Proc. 12th Int. Conf. Cold Fusion, Yokohama, Japan, November 27–December 2, 2005, World Scientific Pub., Singapore, 2006, p. 108.
[6] K.L. Shanahan, Thermochim. Acta 387 (2002) 95.
[7] K.L. Shanahan, Thermochim. Acta 428 (2005) 207.
[8] E. Storms, Thermochim. Acta 441 (2006) 207.
[9] K.L. Shanahan, Thermochim. Acta 441 (2006) 210.
[10] D.M. Rowe (Ed.), CRC Handbook of Thermoelectrics, CRC Press, Boca Raton, 1995 (Section D).
[11] Z.-L. Zhang, M.-H. Zhong, F.-M. Liu, F.-P. Zhong, F. Wu, J. Power Sources 70 (1998) 276.
[12] Y. Saito, J. Power Sources 97–98 (2001) 688.